DYNAMIC PROPERTIES OF SOME GIMBAL AND TEETERING TWO-BLADE HELICOPTER ROTOR HEADS

Alessandro Croce, Radek Possamai, Lorenzo Trainelli
Politecnico di Milano, Milano, Italy

Abstract

The primary aim of the paper is the characterization of the dynamic behaviour of an innovative two-blade main rotor design under cyclic perturbations. The consequent 'wobbling' motion, *i.e.* the 2/rev precession of the hub with respect to the mast, is known as a significant drawback of typical current two-blade rotor realisations, based on a teetering mount, as it induces considerable oscillating loads to the fuselage. As an alternative capable to alleviate this problem, the proposed design is based on a constant-speed gimbal mount. The performance of this solution is contrasted with a pure teetering one, as well as with intermediate architectures retaining only a part of the innovative elements of the new gimbal rotor, in order to appreciate their effects separately. All models are simulated within a high-fidelity finite element multibody framework. The results confirm the superior characteristics of the constant-speed architecture. The study is completed with a sensitivity analysis of the dynamic response of the proposed rotor model with respect to some important design parameters.

1. INTRODUCTION

The present paper aims to characterise the dynamic behaviour of an innovative two-blade main rotor design conceived as a convenient alternative to the standard teetering-type designs employed in current lightweight helicopters. It is well known that these rotors, with their remarkable design simplicity, suffer from some limitations and drawbacks. Among these, one of the most important is related to the vibratory loads transferred to the fuselage as a result of rotor cyclic flapping. This is the typical condition encountered in forward flight or while hovering under gust conditions, and involves a considerable impact on pilot workload, passenger comfort, vehicle handling qualities, and structural fatigue.

In an effort to alleviate this problem, Dr. Vladimiro Lidak (1944-2012), a missed Italian rotorcraft designer and inventor, conceived an innovative rotor head solution based on a homokinetic gimbal mount. This patented design [1] is currently developed by K4A S.p.A., a start-up helicopter manufacturer based in Naples, Italy, to be implemented in the KA-2HT two-seat helicopter.

In order to analyse the dynamic behaviour of this solution, in this paper four different two-blade rotor models fitting the same general requirements for a 650 kg MTOW class helicopter are considered and compared. The main characteristic of the dynamic response to cyclic perturbations, be it pilot control or wind gusts, is the 'wobbling' motion, *i.e.* the precessional 2/rev (two periods per rotor revolution) oscillations of the rotor head entailing analogous variations in the aerodynamic and inertial rotor forces. A thorough comparison of the wobbling behaviour is carried out contrasting Lidak's design with a basic teetering rotor head and variations thereof. Following this analysis, some parametric studies are carried out in order to determine the sensitivity of Lidak's design to important design parameters. The present results are also commented in relation to those presented in a previous work for the same rotor model [2].

2. MULTIBODY SIMULATION

The present study has been conducted by the implementation of high-fidelity aero-servo-elastic models of the various rotor systems within the Cp-Lambda (Code for Performance, Loads and Aeroelasticity by Multi-Body Dynamic Analysis) software. This is based on a state-of-the-art finite-element multibody formulation [3] employing Cartesian coordinates for the description of all entities in the model, while all degrees of freedom are referred to a single inertial frame. The formulation handles arbitrarily large three-dimensional rotations and makes use non-conventional, unconditionally stable time-integration methods [4]. The software has been thoroughly employed in the aero-servo-elastic analysis of rotorcraft systems as well as wind turbine generator systems, e.g. [5, 6, 7].

Structural elements can be modelled as rigid bodies, beams and shells, and joint models. In particular, the blades, as well as other slender linkages, are modelled using geometrically exact, composite-ready beams of arbitrary geometry and accounts for axial, shear, bending and torsional stiffness. Joints are modelled through holonomic or nonholonomic constraints enforced by means of Lagrange multipliers and can account for backlash, free-play and friction.

Lifting lines based on classical two-dimensional blade element theory, accounting for the aerodynamic centre offset, twist, sweep, and unsteady corrections, can be associated with beam elements. Their geometric description is given in terms of three-dimensional twisted curves. At a number of span-wise stations along each lifting line, the aerodynamic characteristics of the aerofoil corresponding to each location are given using look-up tables, which store the values of the sectional lift, drag, and moment coefficients as functions of the local angle of attack, Reynolds and Mach numbers.

An inflow element can be associated with the lifting lines so as to model the rotor inflow effects. The code implements the Peters–He dynamic inflow wake model [8], as well as a classical blade-element momentum (BEM) model based on the annular stream-tube theory with wake swirl. Tip and hub loss models are also considered.

3. ROTOR HEAD MODELS

As mentioned above, the study of the dynamic response to cyclic perturbations of Lidak's gimballed rotor is carried out by a comparison with other reference two-blade architectures. Four different rotor head designs are investigated. Two are based on a configuration involving a constant-speed gimbal mount, allowing two degrees of freedom to the relative motion between hub and mast, referred to as teetering (*i.e.* rotation about an axis normal to both the mast and the blade axis) and feathering (*i.e.* rotation about the blade axis). The other two implement a more classical, much simpler mount, which only permits the teetering single degree of freedom. In this configuration, the rotor head is suspended on the mast by a revolute joint, the teetering hinge. This is by far the most represented configuration in lightweight helicopters, such as the popular Robinson R-22 [9], and will be referred to as the T1 model.

Lidak's design, referred to as the H1 model, is illustrated in Figure 1. It includes also a Bell-Hiller-type flybar fixed to the hub and a complex linkage realizing a 'mixed control' strategy for blade pitching. This consists in the combination of a 'primary', or 'direct' command provided by the pilot through a swashplate and transmitted by pitch links up to a 'mixer'. This element also receives mechanical input by the flybar, the 'secondary' or 'indirect' command. As a consequence, the blades are feathered by a combination of the two control actions, which is delivered by the pitch horns connecting the mixer to the blade root. The resulting cyclic pitch command is given by $\theta = \tau_p \theta_{sw} + (1 - \tau_p) \eta$, where θ_{sw} is the swashplate tilt, η is the hub feathering angle, and τ_p is the primary command ratio.

In order to appreciate the contribution of the gimbal joint and the mixed pitch control to the dynamic

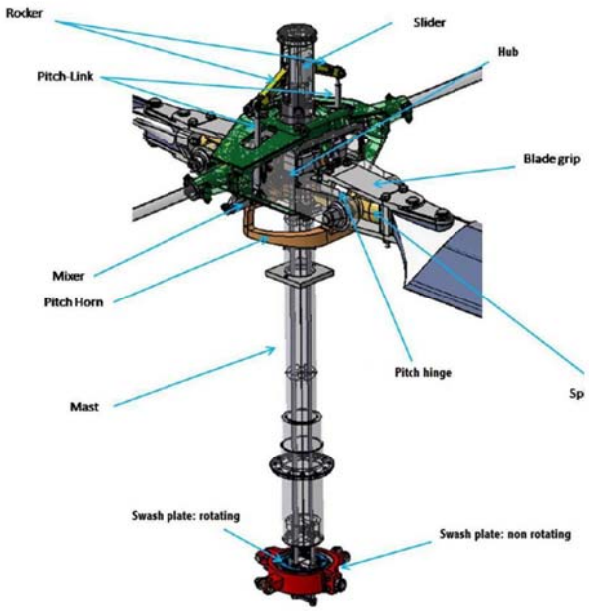

Figure 1. CATIA model of the shaft-rotor head assembly considered in this work (courtesy of K4A S.p.A.).

response of Lidak's rotor head, a 'degraded' version of this design is also investigated. This H2 model features a traditional direct pitch control, without any contribution from the flybar dynamics.

Similarly, in an effort to ascertain the influence of a flybar upon the dynamic response, we also considered an augmentation of the basic teetering design by adding a Bell-type stabilizing bar, free to tilt about an axis fixed to the mast and at right angles with the teetering axis. No contribution to pitch control is considered in this case, referred to as the T2 model.

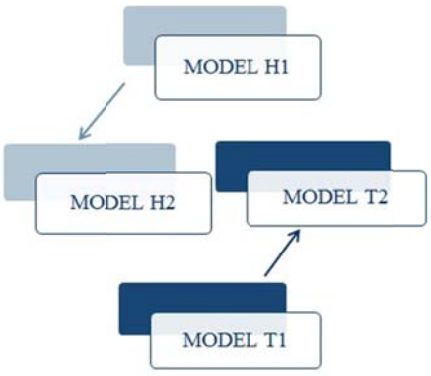

Figure 2. The four rotor head models investigated in this work.

Figure 2 summarizes the relationships between the four architectures. All of them have been equipped with the same set of blades, representative of those considered for the KA-2HT. In the following, these rotor models and their multi-body idealization are descripted.

3.1. Model H1

The H1 rotor head is described in detail in the companion paper [10]. Here, some of its most prominent features are recalled for the sake of convenience. The rotor head is characterized by an original homokinetic gimbal joint connecting the rotor hub to the mast. This is composed of a sequence of revolute pairs mutually arranged at right angles, further constrained in their relative motion by scissor-like mechanisms called bisectors. The latter are crucial to the quasi-constant-speed behaviour of the transmission from the mast to the hub, *i.e.* the attempt to preserve the value of the angular velocity in spite of the relative tilt between the two elements. This complex arrangement enforces a nearly constant ratio of the relative rotations between the internal elements of the gimbal mount. In fact, the bisector pin axis actually bisects the angle formed by the mast and the hub axis normal to the rotor plane, thus approximating an ideal homokinetic transmission.

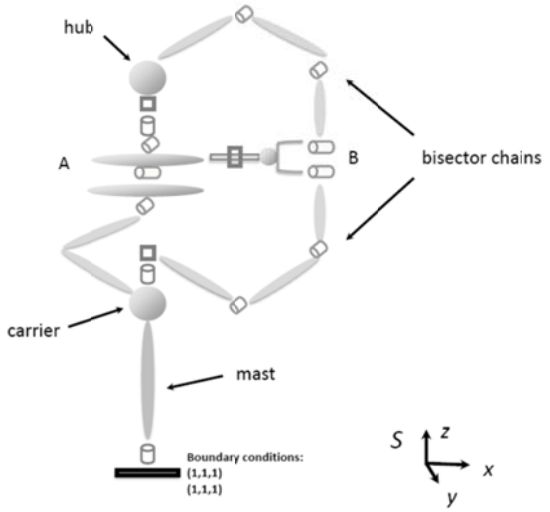

Figure 3. Topological sketch of the H1 rotor-head transmission subsystem.

Figures 3 and 4 represent the multibody implementation of this innovative solution, separated in the rotor head transmission and the pitch control chain subsystems for the sake of clarity. The resulting model includes 59 rigid bodies, 21 beam elements, and 44 joints, for a total number of 1756 degrees of freedom.

3.2. Model H2

The H2 rotor head is derived from the H1, by eliminating the mixed pitch control mechanism. In fact, the pitch links directly actuate the pitch horns, without any contribution from the flybar. With respect to Figure 4, the H2 model is obtained by erasing the connecting elements from the flybar to the pitch horn (starting at point C) and connecting the latter directly to the pitch link (descending from point A). In this way, the flybar motion (*i.e.* the hub feathering) does

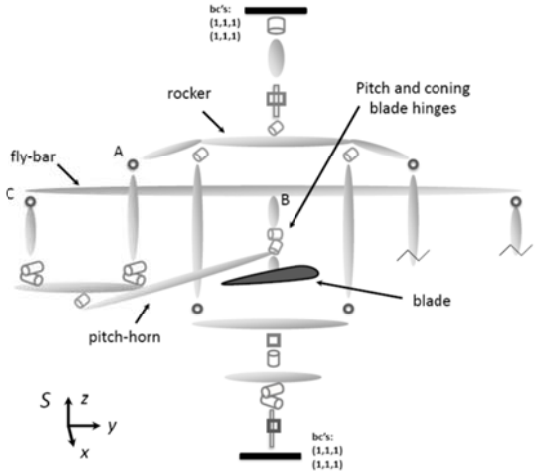

Figure 4. Topological sketch of the H1 model control chain subsystem.

not influence the blade pitch. However, it retains the important function of developing the forces that actuate the hub feathering motion needed to insure the proper behaviour of the gimbal joint.

3.3. Model T1

The T1 rotor head is the simplest realization considered for two-blade helicopter rotors (Figure 5). The rotor head is provided with a central single axis teetering hinge allowing rigid blade flapping with respect to the mast. The model does not include a flybar, and naturally involves only a direct pitch control. The T1 model retains all geometric, inertial and aerodynamic characteristics of H1 and H2 models.

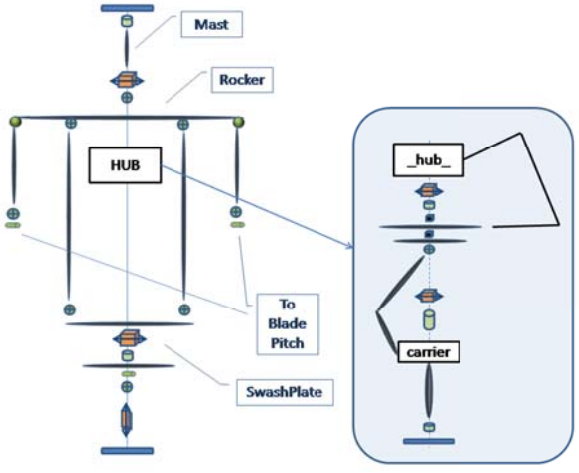

Figure 5. Topological sketch of the T1 model.

3.4. Model T2

The T2 rotor head consists in a modification of the T1 model, with the addition of a Bell-type flybar. The latter is a stabilizing device connected to the mast by means of a revolute joint that allows its tilting movement around an axis at right angles with the mast and the teetering axis. In the present case, the

flybar is the same used in the H1 model, including inertial and aerodynamic properties (but without any mechanical linkage contributing to pitch control), so that the flybar acts also as a damping device.

4. COMPARATIVE WOBBLING ANALYSIS

As a first assessment of the dynamic behaviour of the considered four rotor head models, a wobbling analysis with the Cp-Lambda code has been performed. The angular velocity for all rotor models is 504 rpm. All the time-marching dynamic analyses start from a steady-state hovering condition corresponding to the same rotor thrust (equal to the helicopter's weight, 6400 N) and proceed with a given cyclic perturbation.

4.1. Cyclic command perturbation

In the first set of simulations, the perturbation from hover is realised as step inputs of longitudinal cyclic command which tilt the swashplate from zero to 5° and finally to 10°. After command application, a suitable time lapse is provided to allow the rotor reach periodic conditions.

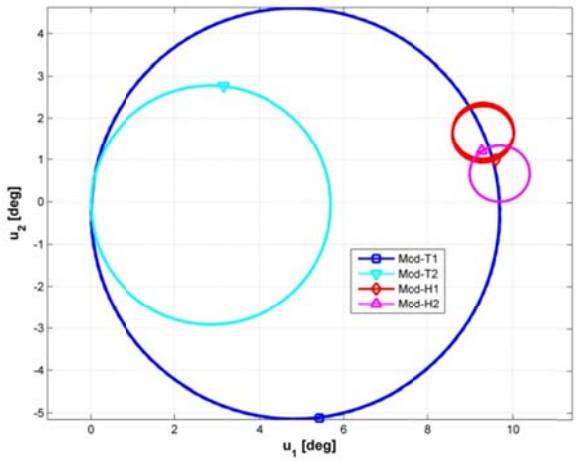

Figure 6. Hub wobbling in a periodic condition with 10° swashplate longitudinal tilt for the T1 (blue), T2 (cyan), H1 (red) and H2 (magenta) models.

Figure 6 shows the hub wobbling for the periodic conditions corresponding to a 10° swashplate longitudinal tilt, for the four models. The trajectories are drawn in the plane of the angles u_1 and u_2, which represent the hub longitudinal and lateral tilt angles with respect to fuselage-fixed axes.

It can be observed that the hub motions for both the teetering models, T1 and T2, describe large circular trajectories passing through the origin (*i.e.* the mast axis). The reduction in the amplitude of the wobbling of model T2 with respect to model T1 is the result of the presence of the flybar. On the other hand, the constant-speed models, H1 and H2, are characterised by much smaller wobbling oscillations.

The precession in this case reaches periodic conditions in the vicinity of the value u_1 = 10°, which means that the average hub longitudinal tilt is approximately the same as that of the swashplate, with a residual amount of average lateral tilt. The differences between models H1 and H2 are very limited, and involve only the average values for u_1 and u_2, while the amount of the wobbling amplitude is substantially the same. The absence of the pitch mixing mechanism induces a lower value of average lateral tilt and a slight higher value of the average longitudinal tilt. We remark that the difference in wobbling between model T1 and model H1 and H2 is strikingly evident, with amplitude values passing from 5° to less than 1°, showing the effectiveness of the constant-speed gimbal solution.

By comparing the model H1 response with the results of [2], we can appreciate significant differences related to the dissimilarity in modelling. In fact, the use of a simplified model plus the assumptions of an ideal homokinetic joint leads to the absence of wobbling in analogous conditions.

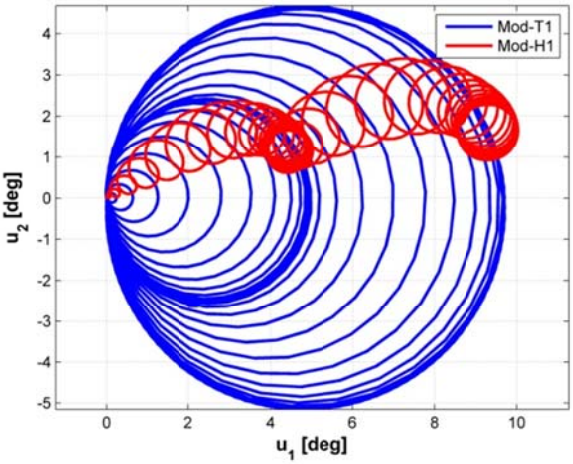

Figure 7. Hub wobbling evolution for two subsequent perturbations of 5° swashplate longitudinal tilt for the T1 (blue) and H1 (red) models.

As a further confirmation, Figure 7 shows the wobbling motion of models H1 and T1 during the full dynamic transient from null cyclic to 5° , followed by a second application of a variation of 5° in longitudinal pitch command. Model H1 shows a lower wobbling amplitude throughout the manoeuvre, involving a certain amount of average lateral tilt. As apparent, the behaviour of model T1 appears much simpler, with a progressive increase in average longitudinal tilt, at null lateral tilt.

In addition to hub motion, several other quantities have been analysed to characterise the four rotor models. Figure 8 refers to the wobbling of the mast resultant internal force vector, which represents the loading imposed by the rotor to the airframe, for the same conditions as Figure 6. Again, the teetering models present larger amplitudes with respect to the

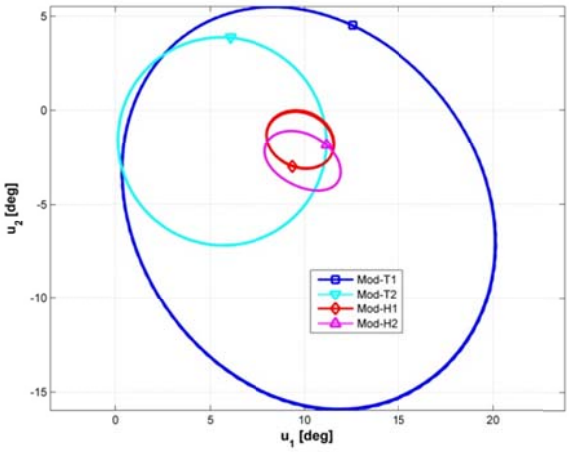

Figure 8. Wobbling of the mast internal force in a periodic condition with 10° swashplate longitudinal tilt for the T1 (blue), T2 (cyan), H1 (red) and H2 (magenta) models.

constant-speed models. The elliptic orbits reflect the complex coupling of rotor aerodynamic and inertial effects contributing to the mast loading. Interestingly, the force oscillations for model T1 show a doubled amplitude with respect to the hub oscillations. In addition, the force response of model T1 involves a higher average lateral tilt than constant-speed models.

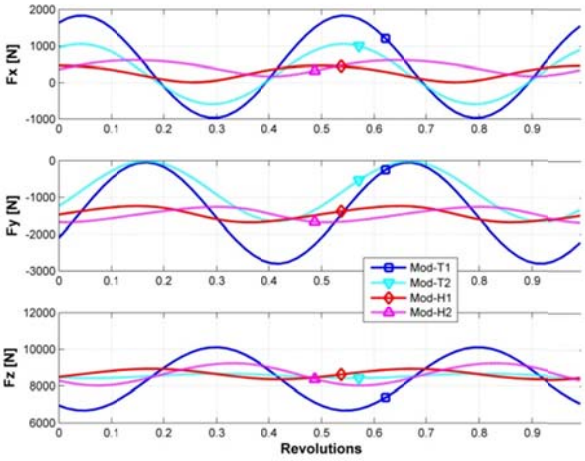

Figure 9. Time histories of the components of the mast internal force in a periodic condition with 10° swashplate longitudinal tilt for the T1 (blue), T2 (cyan), H1 (red) and H2 (magenta) models.

Figures 9 and 10 show the time histories of the mast internal force and moment components, evaluated with respect to fuselage-fixed axes (*z* being the mast axis) within one revolution in periodic conditions. Again, the wide difference in the amplitude values between the different models is apparent, confirming the superior behaviour of the constant-speed solutions.

Figure 11 allows appreciating the transient behaviour within the complete manoeuvre involving the 5° and 10° pitch command applications. Again,

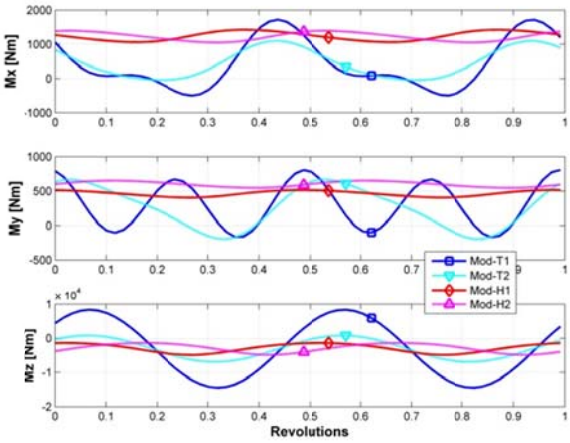

Figure 10. Time histories of the components of the mast internal moments in a periodic condition with 10° swashplate longitudinal tilt for the T1 (blue), T2 (cyan), H1 (red) and H2 (magenta) models.

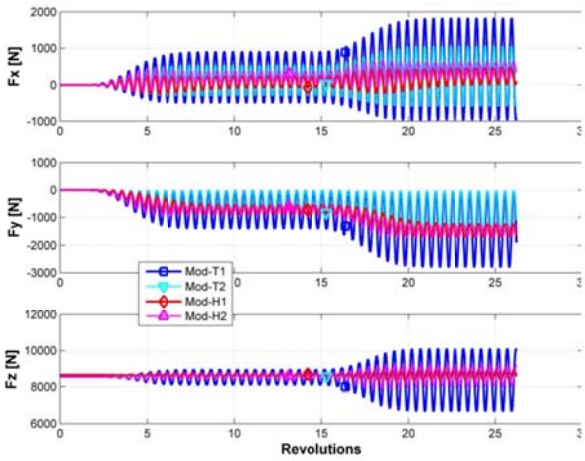

Figure 11. Time histories of the components of the mast internal force for two subsequent perturbations of 5° swashplate longitudinal tilt for the T1 (blue), T2 (cyan), H1 (red) and H2 (magenta) models.

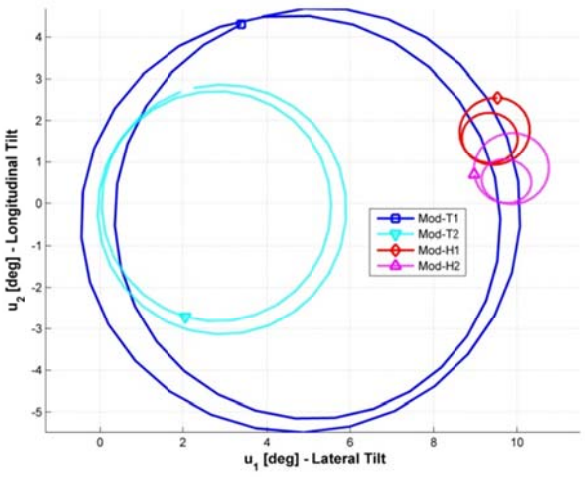

Figure 12. Wobbling of the rotor aerodynamic force in a periodic condition with 10° swashplate longitudinal tilt for the T1 (blue), T2 (cyan), H1 (red) and H2 (magenta) models.

the constant-speed models show lower oscillations throughout the simulation.

The resultant aerodynamic force generated by the rotor was also investigated. As seen in Figure 12, for this quantity a different result is obtained, in that the periodic conditions not only induce a 2/rev component as seen for hub motion and mast internal forces, but also a 1/rev component. This appears as a doubled orbit in the (u_1,u_2) plane, as a result of a single rotor revolution.

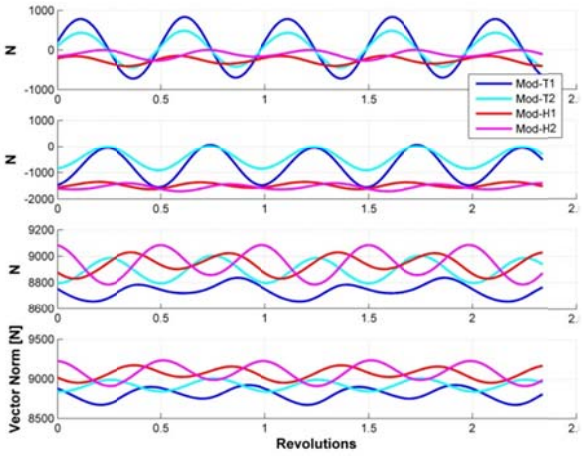

Figure 13. Time histories of the components (above) and the magnitude (below) of the rotor aerodynamic force in a periodic condition with 10° swashplate longitudinal tilt for the T1 (blue), T2 (cyan), H1 (red) and H2 (magenta) models.

This characteristic can be appreciated in Figure 13, where the time histories of the resultant aerodynamic force components are shown, evaluated after reaching periodic conditions.

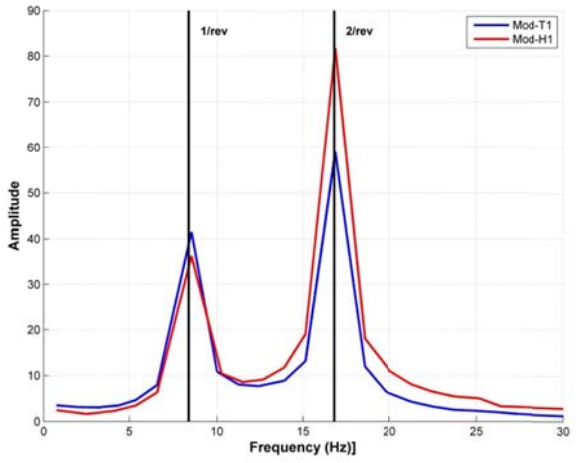

Figure 14. FFT of the magnitude of the rotor aerodynamic force in a periodic condition with 10° swashplate longitudinal tilt for the T1 (blue) and H1 (red) models.

Figure 14 shows the Fast Fourier Transform (FFT) of the time histories of the resultant aerodynamic force magnitude for models T1 and H1. The two signals display a significant 1/rev component along with the 2/rev one. This is not the case when analysing the hub wobbling, as seen in Figure 15, which show only the 2/rev harmonic component.

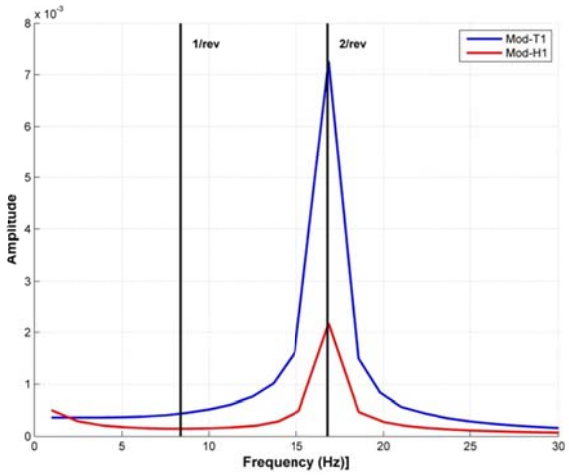

Figure 15. FFT of the magnitude of the rotor aerodynamic force in a periodic condition with 10° swashplate longitudinal tilt for the T1 (blue) and H1 (red) models.

To complete the illustration, Figure 16 is included, in order to grasp the shift between the wobbling trajectories of the hub and of the aerodynamic force vector. It is seen that the motion is approximately similar, so that in all cases the aerodynamic force is almost perpendicular to the hub plane, with somewhat lower variations for constant-speed models.

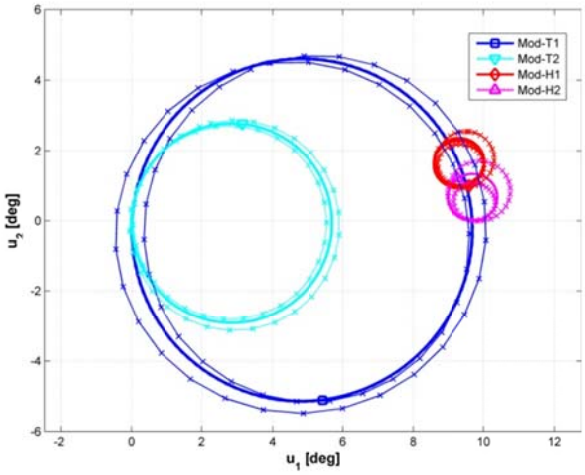

Figure 16. Wobbling of the hub and of the rotor aerodynamic force in a periodic condition with 10° swashplate longitudinal tilt for the T1 (blue), T2 (cyan), H1 (red) and H2 (magenta) models. Hub trajectories are represented by thicker lines, aerodynamic force by thinner lines with 'x' markers.

4.2. Advance ratio perturbation

The second set of simulations considers a step perturbation in the asymptotic wind speed from null (hover) to 20 m/s, which corresponds to an advance

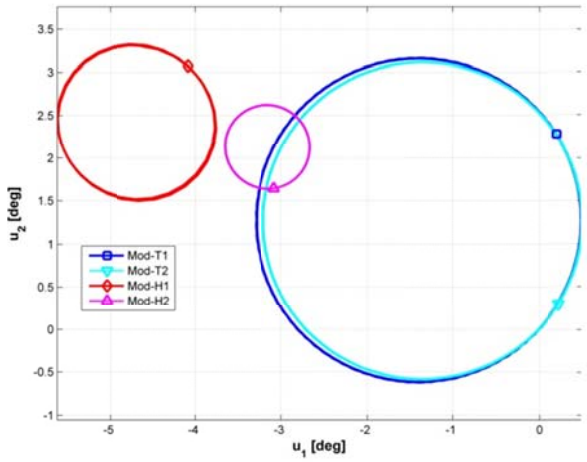

Figure 17. Hub wobbling in a periodic condition with 0.1 advance ratio for the T1 (blue), T2 (cyan), H1 (red) and H2 (magenta) models.

ratio μ = 0.1, in the longitudinal direction. After perturbation, a suitable time lapse is provided to allow the rotor reach periodic conditions.

Figure 17 shows the hub wobbling for the periodic conditions corresponding to μ = 0.1, for the four models. As seen in the case of cyclic perturbation, the hub motions for both the teetering models, T1 and T2, describe larger trajectories passing through the origin, while both constant-speed models, H1 and H2, feature significantly lower amplitude oscillations. It is observed that, at variance with the cyclic perturbation case, the response of models T1 and T2 is extremely similar, while that of models H1 and H2 is markedly different, with an advantage in amplitude reduction for model H2. In this instance, model H1 oscillates about an average tilted position which is the farther away from the initial trim, *i.e.* the origin in the (u_1,u_2) plane.

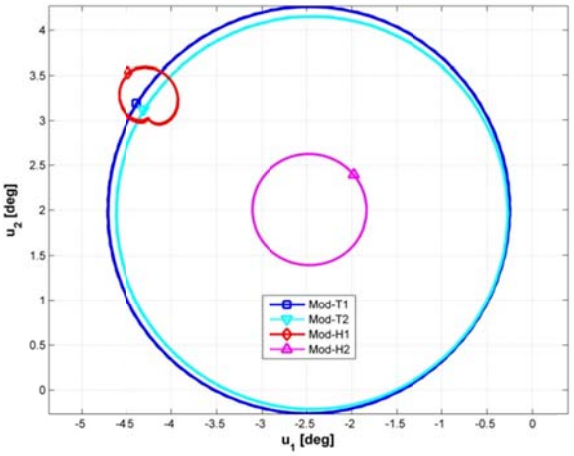

Figure 18. Wobbling of the mast internal force in a periodic condition with 0.1 advance ratio for the T1 (blue), T2 (cyan), H1 (red) and H2 (magenta) models.

Figure 18 refers to the wobbling of the mast resultant internal force vector. In the present case, it is confirmed that the constant-speed models are very effective in reducing the 2/rev loads transferred to the mast, with a superior position for the H1 model.

5. PARAMETRIC STUDIES

In an effort to further characterise the dynamic behaviour of model H1, parametric studies have been carried out to assess the impact of variations in some design parameters. These studies involved the inertial and aerodynamic characteristics of the flybar, the pitch mixing ratio, and the gimbal stiffness.

5.1. Flybar inertia

The first parametric study was focused on the variation of the wobbling response with respect to different values for the flybar inertia J_{fb}. This parameter has a significant role on the feathering dynamics through the flybar Lock number $\gamma_{fb} = 2\,\rho\,a_{fb}\,S_{fb}\,(R_{fb})^3/J_{fb}$, where ρ represents the air density, a_{fb} the lift-curve slope of the flybar paddle, S_{fb} the flybar paddle reference surface, and R_{fb} the flybar paddle reference radius. A sensitivity study was conducted by using the value $J_{fb} = nJ_{ref}$ with n = 1, 2, 3, 4, 5, where J_{ref} denotes its reference design value.

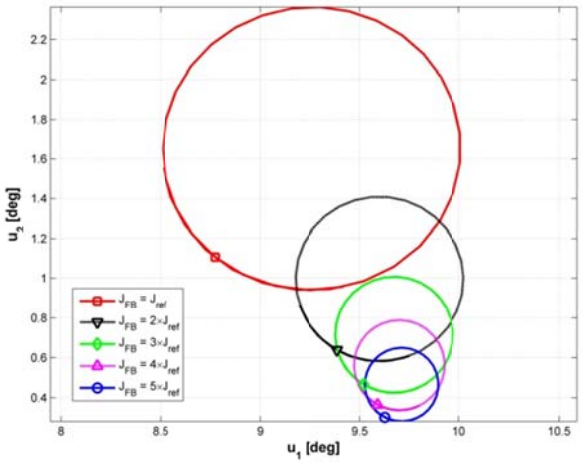

Figure 19. Hub wobbling in a periodic condition with 10° swashplate longitudinal tilt for model H1 with different values of the flybar inertia.

Figure 19 shows the hub wobbling in periodic conditions with a 10° swashplate longitudinal tilt. As it can be seen, the result of an increase in the flybar inertia induces a reduction of the wobbling amplitude and a trend for the average hub tilt angles towards the values of the swashplate tilt angles.

This is clearly seen in Figure 20, where the average value for u_1 tends to increase towards 10°, while the average value of u_2 tends to vanish, as does the wobbling amplitude. This phenomenon seems to hint

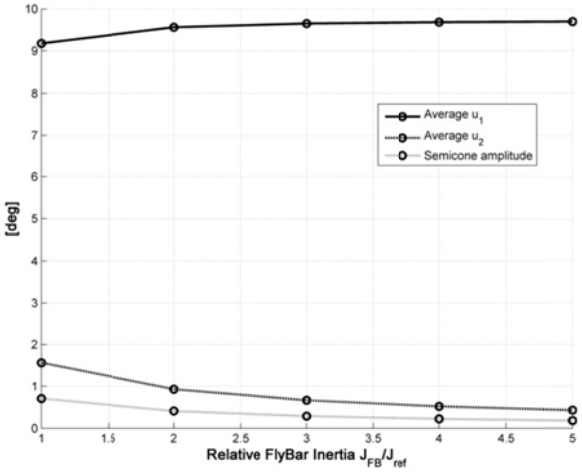

Figure 20. Sensitivity of average tilt angles and wobbling amplitudes with respect to flybar inertia..

that a design employing the same gimbal mount, but featuring four blades, instead of two blades and a flybar, may be conceived to achieve extremely accurate constant-speed transmission performance.

5.2. Flybar aerodynamics

In this section, a variation in the flybar lift-curve slope a_{fb} is considered, as another term included in the flybar Lock number. For this study, we considered variations of ±5% and ±10% of the reference design value and simulated the manoeuvre with 10° swashplate longitudinal tilt, obtaining Figure 21.

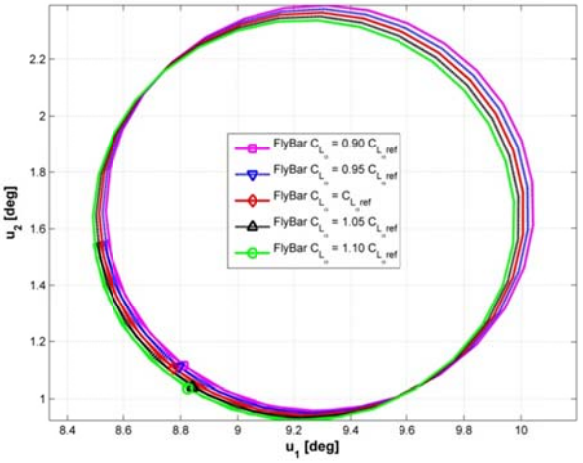

Figure 21. Hub wobbling in a periodic condition with 10° swashplate longitudinal tilt for model H1 with different values of the flybar lift-curve slope.

As apparent, the impact of this parameter is relatively limited for the values considered. An increase in the flybar lift-curve slope determines a displacement of the wobbling axis towards lower values of longitudinal and lateral tilts, and vice-versa. The wobbling amplitude appears unaffected by these variations.

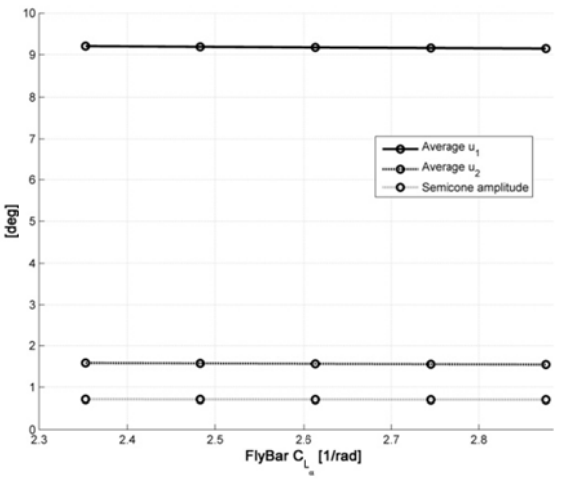

Figure 22. Sensitivity of average tilt angles and wobbling amplitudes with respect to flybar inertia.

Figure 22 reports the slowly varying trends for the average values of u_1 and u_2, and the wobbling amplitude as functions of flybar lift-curve slope.

5.3. Control mixing

An important design parameter of Lidak's design is represented by the pitch mixing, represented by the primary command ratio τ_p. To evaluate the sensitivity of the wobbling response to this parameter, we considered variations of ±5% and ±10% of the reference design value and repeated the simulations leading to periodic conditions at 10° swashplate longitudinal tilt.

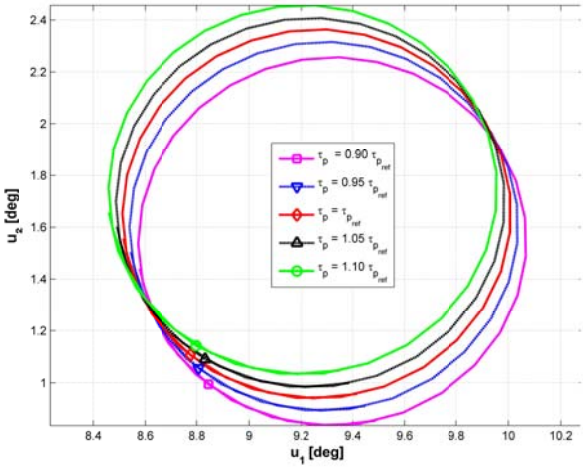

Figure 23. Hub wobbling in a periodic condition with 10° swashplate longitudinal tilt for model H1 with different values of the pitch mixing ratio.

Figure 23 illustrates the wobbling trajectories for the considered variations. Here, the relative influence of the parameter variation again appears relatively limited. An increase in the mixing ratio (*i.e.* enlarging the influence of the primary command upon the blade pitch, at the expense of the influence of the secondary command) determines a displacement of

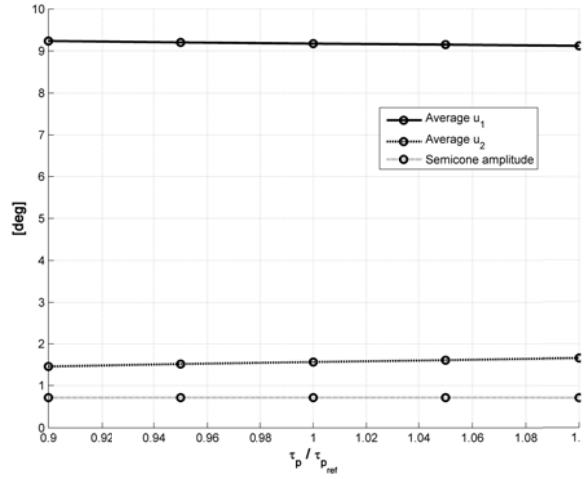

Figure 24. Sensitivity of average tilt angles and wobbling amplitudes with respect to pitch mixing ratio.

the wobbling axis towards lower values of longitudinal tilt and higher values of lateral tilt, and vice-versa. Again, the wobbling amplitude appears unaffected by these variations.

Figure 24 reports the slowly varying trends for the average values of u_1 and u_2, and the wobbling amplitude as functions of pitch mixing ratio.

5.4. Gimbal stiffness

The last parametric study considered the gimbal stiffness. This parameter was not considered in the comparative studies discussed above, for the sake of simplicity in contrasting constant-speed and teetering rotor models. However, the design conceived for the KA-2HT helicopter includes torsional stiffness within the gimbal joint, as a way to improve control power in low-*g* flight conditions. The torsional springs have different values K_f about the feathering axis and $K_t = 2\ K_f$ about the teetering axis. The reference design value for K_f is K_{ref} = 3610 Nm/rad. We performed the usual dynamic simulations with values of K_f in a range from 0 to 100% of K_{ref} with 10% increments, preserving the ratio between K_f and K_t.

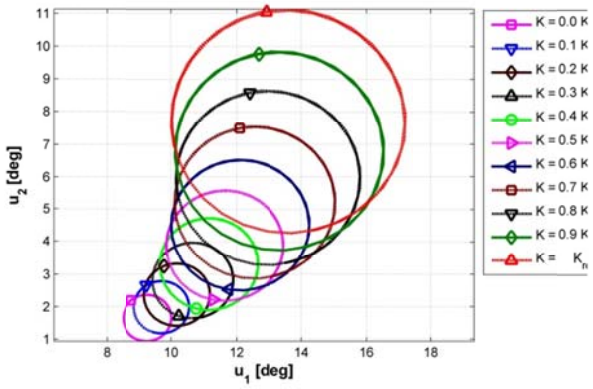

Figure 25. Hub wobbling in a periodic condition with 10° swashplate longitudinal tilt for model H1 with different values of the gimbal stiffness.

As seen in Figure 25, the gimbal stiffness impacts significantly on the wobbling response in terms of both average values and amplitude. In fact, increasing the gimbal stiffness induces larger oscillations about an axis which is longitudinally displaced beyond the swashplate tilt value. Also, lateral displacement becomes very important.

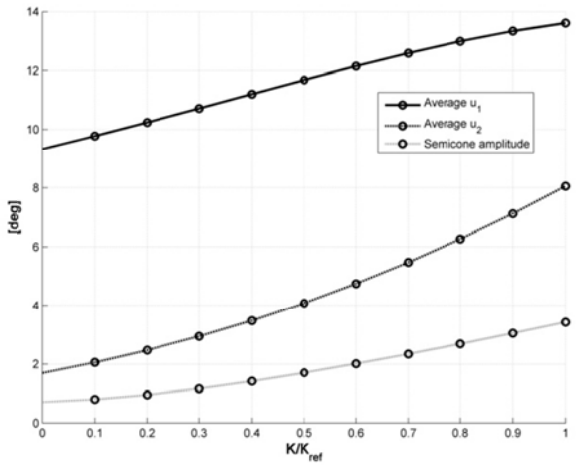

Figure 26. Sensitivity of average tilt angles and wobbling amplitudes with respect to gimbal stiffness.

Figure 26 shows the rapidly varying trends for the average values of u_1 and u_2, and the wobbling amplitude as functions of the gimbal stiffness.

6. CONCLUDING REMARKS

In this paper, a study of the dynamic behaviour of four different main rotor models designed for two-blade lightweight helicopters, two of the teetering type and two of a gimbal type, has been carried out. The gimbal models are the novel design described in detail in [10] and a variation of the same design without pitch command mixing. Both feature an innovative constant-speed transmission between mast and hub. The typical response to cyclic perturbations of all these rotors, a 2/rev precession of the hub with respect to the mast, has been simulated by means of a high-fidelity finite element multibody formulation. This allows to accurately simulate the complexity in the rotor responses when subjected to cyclic pitch input or advance ratio perturbations. The analysis has been based on hub trajectory, internal mast forces and moments, and resultant rotor aerodynamic force. In all cases, the superiority of the constant-speed types is apparent. Motivated by this result, a sensitivity analysis for the constant-speed design has been performed, assessing the impact of variations in flybar inertia, flybar lift-curve slope, pitch command mixing ratio and gimbal stiffness. It is observed that the flybar inertia and gimbal stiffness can significantly vary the wobbling response, both in terms of average tilt values and amplitude.

7. REFERENCES

[1] Lidak V., "Constant Velocity Joint for Helicopter Rotors", patent WO/2010/128378/ A2, 2010.

[2] Avanzini G., De Matteis G., Lucertini F.F., Torasso A., "Dynamic behaviour and Response of a Two-Bladed Gimballed Rotor", 36th European Rotorcraft Forum (ERF 2010), Paris, France, September 2010.

[3] Bauchau O.A., Bottasso C.L., Nikishkov Y.G., "Modeling Rotorcraft Dynamics with Finite Element Multibody Procedures", *Mathematical and Computer Modelling*, **33**, 1113-1137 (2001).

[4] Bauchau O.A., Bottasso C.L., Trainelli L., "Robust Integration Schemes for Flexible Multibody Systems", *Computer Methods in Applied Mechanics and Engineering*, **192**: 395–420 (2003).

[5] Bottasso C.L., Trainelli L., Abdel-Nour P., Labò G., "Tilt Rotor Analysis and Design Using Finite-Element Multibody Dynamics", 28th European Rotorcraft Forum (ERF 2002), Bristol, UK, September 2002.

[6] Bottasso C.L., Croce A., Leonello D., Riviello L. , "Steering of Flexible Multibody Models with Application to the Simulation of Maneuvering Flight", 4th European Congress on Computational Methods in Applied Sciences and Engineering (ECCOMAS 2004), Jyväskylä, Finland, July 2004.

[7] Bottasso C.L., Croce A., Savini B., Sirchi W., Trainelli L., "Aeroelastic Modeling and Control of Wind Turbine Generators Using Finite Element Multibody Procedures", *Multibody System Dynamics*, **16** (3): 291-308 (2006).

[8] Peters D.A., He C.J., "Finite state induced flow models. Part II: Three-dimensional rotor disk", *Journal of Aircraft*, **32**: 323–333 (1995).

[9] http://www.robinsonheli.com/rhc_r22_beta_ii.html (retrieved July 2014)

[10] Croce A., Possamai R., Savorani A., Trainelli L., "Modelling and characterization of a novel gimbal two-blade helicopter rotor", 40th European Rotorcraft Forum (ERF 2014), Southampton, UK, September 2014.